International Journal of Nanomedicine

Dovepress
open access to scientific and medical research

Open Access Full Text Article

ORIGINAL RESEARCH

The Stability of Dentin Surface Biobarrier Consisting of Mesoporous Delivery System on Dentinal Tubule Occlusion and Streptococcus Mutans Biofilm Inhibition

Jian Yu*
Luyao Yi*
Rui Guo
Jingmei Guo
Hongye Yang
Cui Huang

The State Key Laboratory Breeding Base of Basic Science of Stomatology (Hubei-MOST) & Key Laboratory for Oral Biomedicine Ministry of Education, School and Hospital of Stomatology, Wuhan University, Wuhan, People's Republic of China

*These authors contributed equally to this work

Background: The dentin exposure always leads to dentin hypersensitivity and/or caries. Given the dentin's tubular structure and low mineralization degree, reestablishing an effective biobarrier to stably protect dentin remains significantly challenging. This study reports a versatile dentin surface biobarrier consisting of a mesoporous silica-based epigallocatechin-3-gallate (EGCG)/nanohydroxyapatite delivery system and evaluates its stability on the dentinal tubule occlusion and the *Streptococcus mutans* (*S. mutans*) biofilm inhibition.

Materials and Methods: The mesoporous delivery system was fabricated and characterized. Sensitive dentin discs were prepared and randomly allocated to three groups: 1, control group; 2, casein phosphopeptide–amorphous calcium phosphate (CPP–ACP) group; and 3, the mesoporous delivery system group. The dentin permeability, dentinal tubule occlusion, acid and abrasion resistance, and *S. mutans* biofilm inhibition were determined for 1 week and 1 month. The in vitro release profiles of EGCG, Ca, and P were also monitored.

Results: The mesoporous delivery system held the ability to sustainably release EGCG, Ca, and P and could persistently occlude dentinal tubules with acid and abrasion resistance, reduce the dentin permeability, and inhibit the *S. mutans* biofilm formation for up to 1 month compared with the two other groups. The system provided prolonged stability to combat oral adverse challenges and served as an effective surface biobarrier to protect the exposed dentin.

Conclusion: The establishment of the dentin surface biobarrier consisting of a mesoporous delivery system indicates a promising strategy for the prevention and the management of dentin hypersensitivity and caries after enamel loss.

Keywords: epigallocatechin-3-gallate, nanohydroxyapatite, mesoporous silica, dentin, biofilm

Correspondence: Hongye Yang; Cui Huang
The State Key Laboratory Breeding Base of Basic Science of Stomatology (Hubei-MOST) & Key Laboratory for Oral Biomedicine Ministry of Education, School and Hospital of Stomatology, Wuhan University, #237 Luoyu Road, Wuhan, 430079, Hubei Province, People's Republic of China
Email yanghongye@whu.edu.cn; huangcui@whu.edu.cn

Introduction

Nature evolves numerous organisms with delicate structures and excellent functionality, of which the human teeth are among the best examples.[1] As the hardest tissue, the enamel surrounds the outermost layer of the tooth crown and consists primarily of apatite crystals.[2] Owing to the tightly packed arrangement and well-defined orientation of the crystals, the enamel can respond effectively to routine challenges, including thermal, cool, chemical, and mechanical stimuli, serving as a natural

surface barrier for the protection of the underlying dentin and the internal pulp tissue in oral environments.[3,4]

However, the mature enamel is acellular and scarcely self-repairing once damaged or lost.[5] With the disappearance of such a barrier, the underlying dentin will inevitably be exposed. In most cases, in clinical practice, this phenomenon frequently occurs after the tooth preparation during the process of the indirect restoration.[6–9] The unique tubular structure of dentin provides channels for external irritants to trigger several aggravating symptoms or relevant diseases.[10,11] For instance, the movement of the intradentinal fluid induced by tactile, osmotic, thermal, or chemical stimuli can provoke impulse conduction, leading to dentin hypersensitivity.[12] The mineralization in dentin is lower compared to enamel, and coupling with patent orifices allow dental caries to be susceptible and progress rapidly.[13] The frequent invasion of cariogenic bacteria from the dentin to the dental pulp results in pulp inflammation.[14]

Various approaches have been introduced to address these issues over the decades. On the one hand, desensitizing materials, such as adhesives, bioglass, calcium phosphates, and fluorides, aim at blocking dentinal tubules and decreasing the intradentinal permeability (also known as immediate dentin sealing) have emerged on the basis of the classic hydrodynamic hypothesis.[15–18] The stability and the durability of these methods remain limited despite their immediate efficacy because obstructed tubules are generally unreliable for resisting routine acid or abrasion attack in a complicated oral environment for prolonged periods.[19,20] On the other hand, a number of antimicrobial agents, including stannous fluoride, chlorhexidine, triclosan, and silver ions, are designed to eliminate dental biofilm triggered by cariogenic bacteria, especially *Streptococcus mutans* (*S. mutans*).[21–23] Unfortunately, the longevity of such therapies is always compromised due to the incompetence of the tubule sealing to cut off bacterial invasion pathways.[24] Given the nature of the dentin, an effective surface biobarrier after the enamel loss during the process of the indirect restoration should be engineered to stably protect the vulnerable dentin against external adverse challenges.

Since the dentin is mainly composed of apatite crystals, analogous mineral compounds, such as nanohydroxyapatite (nHAp), should be applied for tubule occlusion on the basis of biomimetics.[25] As a green tea extract with high biological activity, the epigallocatechin-3-gallate (EGCG, Figure 1) has exhibited remarkable advantages in inhibiting the biofilm formation of cariogenic bacteria.[26] On account of their unique properties, a biocompatible nanocarrier, mesoporous silica nanoparticles (MSN),[27,28] is used in our previous study to develop the MSN-based delivery system (EGCG-encapsulated nHAp@MSN, EGCG@nHAp@MSN).[29] This system shows an immediate efficacy to block the tubules and suppress the biofilm growth of *S. mutans*. However, whether this system remains effective for providing prolonged stability to overcome oral adverse challenges and prevent the occurrence and progression of related diseases is unknown. An effective surface biobarrier must sustainably protect the exposed dentin after enamel damage and possess reliable stability for tubule occlusion with acid and abrasion resistance and *S. mutans* biofilm inhibition. To the best of our knowledge, no information is currently available concerning this point.

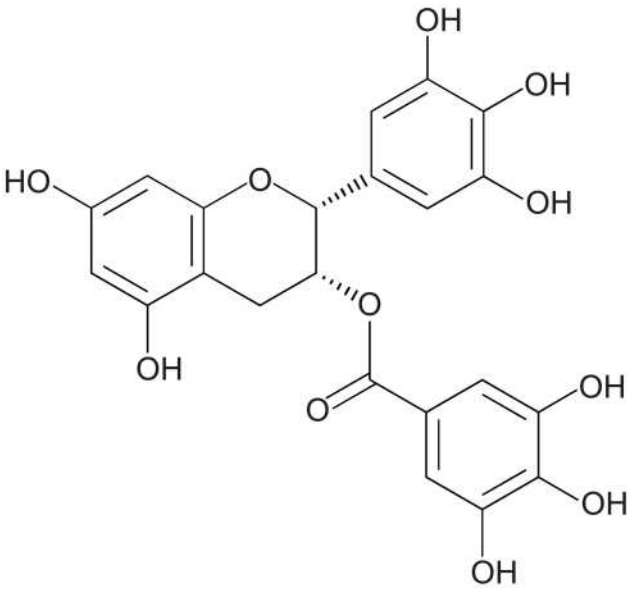

Figure 1 Chemical structure of epigallocatechin-3-gallate (EGCG).

Therefore, this study aims to determine the feasibility of the mesoporous delivery system to serve as a dentin surface biobarrier and evaluate its stability to protect dentin. Three hypotheses are tested in the present study: applying the mesoporous delivery system would 1) achieve dentinal tubule occlusion for 1 month, 2) provide acid and abrasion resistance for 1 month, and 3) retain its ability to inhibit *S. mutans* biofilm formation for 1 month.

Materials and Methods

Materials

All experimental materials were used as received with no purification. MTT kit was purchased from Amresco Inc.

(Solon, OH, USA). Casein phosphopeptide–amorphous calcium phosphate (CPP–ACP) contained commercial paste Tooth Mousse was purchased from GC Corp. (Tokyo, Japan). Brain heart infusion (BHI) and agar powder were obtained from Difco, Becton-Dickinson (Sparks, MD, USA). EGCG, MSN, and dimethyl sulfoxide (DMSO) were acquired from Sigma-Aldrich (St. Louis, MO, USA). Glutaraldehyde, sucrose, citric acid monohydrate, ethylenediamine tetraacetic acid (EDTA), absolute ethanol, and phosphate-buffered saline (PBS) were obtained from Aladdin Bio-Chem Technology (Shanghai, China). Ammonium phosphate [$(NH_4)_2HPO_4$] and calcium nitrate tetrahydrate [$Ca(NO_3)_2{\cdot}4H_2O$] were supplied by Kermel Chemical Reagent (Tianjin, China). Cell Counting Kit-8 (CCK-8) was purchased from Dojindo (Kumamoto, Japan).

Fabrication of EGCG@nHAp@MSN

EGCG@nHAp@MSN, the mesoporous silica-based delivery system, was fabricated based on reported techniques and modified in the recently published paper.[29,30] In brief, the nHAp@MSN was initially synthesized through the dropwise addition of aqueous solutions of $Ca(NO_3)_2{\cdot}4H_2O$ (8 mmol) and $(NH_4)_2HPO_4$ (4.8 mmol, in accordance with the molar ratio of calcium and phosphorus at 1.67) into the MSN suspension (MSN, 0.48 g; deionized water, 20 mL). The mixed suspension was centrifuged, vacuum-dried, and calcined to obtain the nHAp@MSN powder. The EGCG@nHAp@MSN was fabricated by dispersing 100 mg nHAp@MSN powder into the ethanol solution of EGCG with concentration of 2 mg/mL (40 mL). The mixture was constantly stirred for 2 h and vigorously shaken for 72 h. A white precipitate was retrieved by centrifuging the dispersed mixture. After ethanol washing three times, filtering, and vacuum drying, the powdery product of EGCG@nHAp@MSN was ultimately achieved. A JEM-1400Plus transmission electron microscope (TEM, JEOL, Tokyo, Japan) was employed to characterize the ultrastructure of the two powdery products. The surface characteristics of the MSN and the EGCG@nHAp@MSN were analyzed by collecting N_2 adsorption–desorption isotherms using porosimetry (ASAP2020M, Micromeritics, Atlanta, GA, USA). The Brunauer–Emmett–Teller (BET) and Barrett–Joyner–Halenda (BJH) methods were employed to calculate the specific surface areas and pore size distributions, respectively. The powder of nHAp@MSN, EGCG, and EGCG@nHAp@MSN was suspended in deionized water at pH 7.0 and ultrasonically oscillated for 15 min. Their zeta potentials were immediately detected by using a laser particle sizer (Zetasizer Nano ZSP, Malvern Instruments Ltd., Malvern, UK).

Preparation of Dentin Discs

This study was conducted in accordance with the Declaration of Helsinki. After achieving donors' informed consents according to the protocol approved by the Ethics Committee of School and Hospital of Stomatology, Wuhan University [no. 2019 (A11)], sound human third molars were obtained, cleaned, and reserved in thymol solution [0.5% (w/v)] at 4 °C. Dentin disc specimens (1.0 ± 0.1 mm in thickness, 6.0 ± 0.5 mm in diameter) were prepared using a water-cooling, low-speed Isomet diamond saw (Buehler, Lake Bluff, IL, USA) to slice molars below the enamel–dentinal junction, which was parallel to the occlusal plane. These discs were uniformly burnished to 1.0 mm thickness while excluding unqualified ones for minimizing the effect on measuring the dentin permeability.

Design of Experiments

The chief experimental design is summarized in Figure 2. The smear layer was created using the 600-grit SiC sandpaper under water irrigation to polish the occlusal surface of each dentin disc. An aqueous EDTA solution (0.5 mol) at pH 7.4 was immediately prepared. The sensitive tooth model was simulated by immersing each disc into the EDTA solution for 2 min to remove the smear layer and expose the dentin and then thoroughly rinsed.[31] Ninety-six EDTA-etched discs were randomly classified into three groups (n = 32) according to the following surface treatment protocols.

Group 1 (control group): The occlusal surface of the discs was treated by applying sterile deionized water twice with a prophy cup at low speed for 30 s.

Group 2 (CPP–ACP group): The occlusal surface of the discs was treated by applying a CPP–ACP contained Tooth Mousse paste twice with a prophy cup at low speed for 30 s.

Group 3 (EGCG@nHAp@MSN group): The occlusal surface of the discs was treated by applying a slurry of EGCG@nHAp@MSN twice in accordance with the powder/liquid ratio at 10 mg/100 μL (prepared by dispersing the dried powder of the material into sterile deionized water) by using a prophy cup at low speed for 30 s.

The discs from three groups were preserved in artificial saliva (contained 30 mM KCl, 4.0 mM KH_2PO_4, 0.2 mM

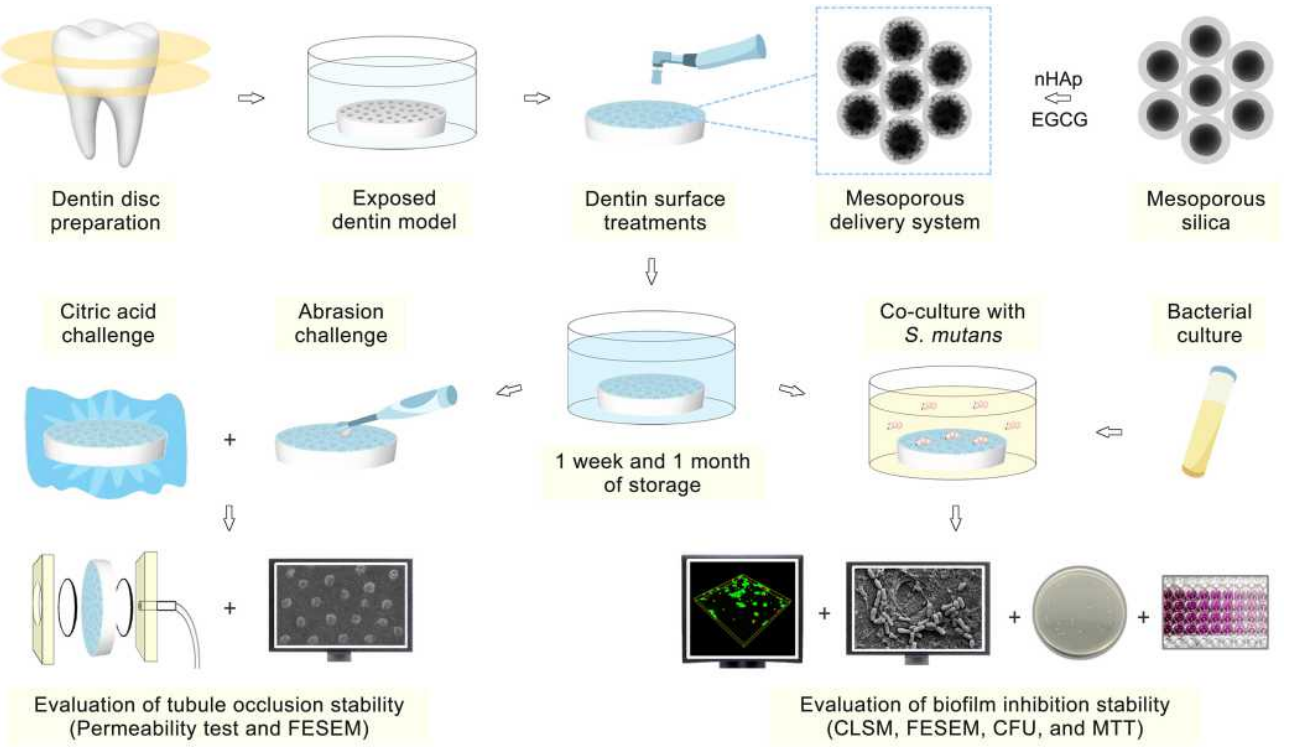

Figure 2 Schematic of the experimental design conducted in the present study.

$MgCl_2 \cdot 6H_2O$, 0.7 mM $CaCl_2$, 0.3 mM NaN_3, and 20 mM HEPES buffer) prepared in line with a previous study at 37 °C (pH 7.4) and replaced every 2 days.[32] After 7 days (1 week) of storage, half of the discs (16 discs) from each group were chosen and randomly classified into two subgroups (n = 8). One subgroup was used to determine the routine acid resistance by soaking the discs into the aqueous citric acid solution [6% (w/v)] at pH 1.5 for 60 s.[19] Another subgroup was used to determine the routine abrasion resistance by brushing the discs with Colgate 360° soft-bristled toothbrush (Colgate-Palmolive Co., Guangzhou, China) for 3 min. A uniform velocity of 150 strokes per min and a constant load of 150 g were adopted, and an inclination angle of 90° on the occlusal surface of each disc was applied by the toothbrush.[19] After 30 days (1 month) of storage, the other half of the discs (16 discs) from each group were randomly classified into two subgroups by using the previously mentioned procedure to determine the routine acid or abrasion resistance.

Assessment of Dentin Permeability

A modified fluid permeation device designed on the basis of our previous research was utilized to assess the dentin permeability.[29] The approximate pulp pressure of 20 cm deionized water was simulated using a water reservoir. For the fluid permeation, the uniform surface area of approximately 0.38 cm^2 was provided by each disc, which was tightly connected to two plexiglass cubes and rubber rings. The flow rate (μL/min) across the discs was individually monitored by following a bubble shifted in a 25 μL microcapillary glass tube. By dividing the flow rate (μL/min) by surface area (cm^2) and simulated pressure (20 cm H_2O), the hydraulic conductance (Lp) was calculated. The Lp values of each disc at different time points (ie, after EDTA etching, surface treatments, citric acid challenge, or abrasion challenge) were recorded. The Lp value derived from the EDTA etching was designated as 100% dentin permeability, and the dentin permeability of each disc at the other time points was expressed as a percentage (Lp%) of the Lp value of 100% permeability.

Tubule Occlusion Examination

The effectiveness of different surface treatments on the tubule occlusion and the acid or abrasion resistance was evaluated using a Sigma Carl-Zeiss field-emission scanning electron microscope (FESEM, Jena, Germany). In accordance with the same procedure as described in the aforementioned sections, 12 dentin discs for each group were prepared and grouped. Prior to the FESEM observation, each disc was longitudinally segmented into two

equal parts according to the approach suggested by Wang et al.[31] One part was used for cross-section examination, and the other part was applied for longitudinal-section examination. After dehydration and sputter-coating by Au–Pd alloy, each disc was surveyed under FESEM, and the representative images were recorded.

Antibiofilm Evaluation of S. Mutans

Specimen Preparation and Biofilm Cultivation

S. mutans (ATCC 25175), the standard strain isolated from carious dentin, was achieved from the School of Stomatology, Wuhan University. After 24 h of anaerobic cultivation in BHI broth at 37 °C, the *S. mutans* suspension was collected. The inoculation medium of *S. mutans* with the concentration at 10^8 CFU/mL was adjusted before usage. In accordance with the same approach as described in the aforementioned sections, additional third molars were sliced to produce 60 qualified dentin discs and subjected to the EDTA etching. The discs were randomly assigned to three groups (control, CPP–ACP, and EGCG@nHAp@MSN groups; n = 20 each) with 2 h of ultraviolet disinfection on each aspect followed by storage in sterile deionized water at 37 °C (half for 1 week of storage, and the other half for 1 month of storage). Twenty discs (10 for a 1-week test, 10 for a 1-month test) from each group were transferred into 24-well plates (NEST Biotechnology, Wuxi, China). Subsequently, 1 mL of *S. mutans* medium supplemented with 1% (w/v) sucrose was injected into each well. After 24 h of biofilm formation under anaerobic environment at 37 °C, all discs were collected. Nonadherent bacteria were gently rinsed away by using sterile PBS, and all discs were placed in another 24-well plate.

CLSM Evaluation

Four discs (two for a 1-week test, two for a 1-month test) in each group were randomly selected, and a Zeiss LSM 510 confocal-laser scanning microscope (CLSM, Jena, Germany) was employed to evaluate the *S. mutans* biofilm formation. Green and red fluorescence were yielded after staining live and dead bacteria with SYTO-9 and propidium iodide for 15 min by using LIVE/DEAD BacLight bacterial viability kits (Kit L 13152, Molecular Probes, Invitrogen, Eugene, OR, USA).[33] By capturing the biofilm images from bottom (attached with the treated surface of each disc) to top, 2 μm z-step images of the two representative z-stacks from each biofilm were obtained. These confocal z-stack images were analyzed by Bitplane Imaris 7.4.2 software (Zurich, Switzerland). To determine the effectiveness of different surface treatments on biofilm inhibition, the z-stacks (20 μm thickness) derived from the first 10 layers were counted in live/dead bacteria biomass distributions.

FESEM Evaluation

Four discs (two for a 1-week test, two for a 1-month test) in each group were randomly chosen and immobilized using 2.5% (w/v) aqueous glutaraldehyde solution for 2 h at 4 °C. After that, the discs were subjected to gradient dehydration by using ethanol, desiccated for 48 h, and Au–Pd alloy sputter coating. The effects of different surface treatments on the *S. mutans* adherence and the biofilm morphology were observed using FESEM.

CFU Evaluation

Six discs (three for a 1-week test, three for a 1-month test) in each group were randomly chosen to determine the inhibitory ability on the *S. mutans* colony reproduction. Each disc was placed in centrifuge tubes containing 3 mL of sterile PBS. The coated biofilm was detached by vortex-mixing for 2 min and subjected to tenfold gradient dilution.[34] Culture dishes (NEST Biotechnology, Wuxi, China) overspread with BHI agar were used by injecting each dilution at 40 mL aliquot. After 24 h of anaerobic cultivation at 37 °C, manual calculation was conducted for counting the total number of colonies from each dish. For each disc in each group, three replicates were performed.

MTT Evaluation

The six remaining discs (three for a 1-week test, three for a 1-month test) in each group were used for monitoring *S. mutans* metabolic activities. The disc in each well was injected by MTT solution (prepared at the concentration of 0.5 mg/mL) with 1 mL. After 4 h of anaerobic cultivation at 37 °C, the supernatant was removed. The disc in each well was then injected with DMSO (1 mL) for dissolving formazan crystals. A Powerwave 340 spectrophotometer (Bio Tek Instruments, Winooski, VT, USA) was employed to detect absorbance. The measuring wavelength was set at 570 nm. For each disc in each group, four readings were performed.

Cytotoxicity Assay

The cytotoxicity of EGCG@nHAp@MSN was assessed using CCK-8 assay. After achieving the donors' informed consents, human dental pulp cells (HDPCs) were acquired from healthy human dental pulp tissues

of premolars for orthodontic extraction. Briefly, the HDPCs were seeded in 96-well plates at 5000 cells/well and cultured for 24 h (5% CO_2, 37 °C) to obtain 80–85% confluency. These cells were then exposed to gradient concentrated EGCG@nHAp@MSN at 0, 250, 500, and 1000 μg/mL. After incubation for 1, 3, and 7 days, 10 μL of CCK-8 solution was added into each well and cultured for 2 h. The optical density at 490 nm was detected by using the spectrophotometer. Background optical density of media was subtracted from the readings. The result was expressed as relative cell viability (%) with regard to a control group only with the culture medium. Experiments were implemented in sextuplicate.

Release of EGCG, Ca, and P

Briefly, 100 mg EGCG@nHAp@MSN was dispersed into 10 mL of sterile deionized water. Under constant shaking at 37 °C in the dark, the released amounts of EGCG, Ca, and P was respectively measured at 1, 3, 7, 14, and 30 days. At each time interval, the suspension was centrifuged at 4000 rpm for 5 min. After that, 1 mL of supernatant was collected and replaced with equal volume of fresh sterile deionized water.[35] An ultraviolet–visible UV-2401 spectrophotometer (Shimadzu, Tokyo, Japan) was employed to measure cumulative EGCG release of these supernatants. The monitoring wavelength of 325 nm was selected. An IRIS Intrepid II inductively coupled plasma-atomic emission spectrometer (ICP-AES, Thermo-Fisher Inc., Waltham, MA, USA) was used to measure cumulative release of Ca and P ions.

Statistical Analysis

All data were directly presented as mean ± standard deviation without preprocessing and calculated in Excel 2016 (Microsoft, Redmond, WA, USA). The statistical analysis was carried out using SPSS 22.0 (IBM, Armonk, NY, USA). After the normal distribution and the equal variance of dentin permeability, CFU, MTT, and CCK-8 data were confirmed, a two-factor (main effect, surface treatment [group]; repeated measurement, time point) repeated-measurement analysis of variance (ANOVA) and post-hoc Tukey's test were conducted for dentin permeability analysis and pairwise comparison. The two-factor (variables: surface treatment [group] and storage time) ANOVA and post-hoc Tukey's test were conducted for CFU and MTT analyses and pairwise comparison. The two-factor (variables: concentration and time) ANOVA and post-hoc Tukey's test were conducted for CCK-8 analysis and pair-wise comparison. Significance level was set at 0.05.

Results

Characterization

The representative TEM image of MSN revealed distinct spherical ultrastructure with diameter of approximately 300 nm, highly ordered mesoporosity, and a channel framework (Figure 3A). The EGCG@nHAp@MSN exhibited a well-maintained spherical morphology with mesoporosities that were not clearly defined after the involvement of nHAp and EGCG (Figure 3B). The surface of MSN was uniformly loaded with nHAp clusters, and the channel framework of MSN was partially obscured by the encapsulation of EGCG into the mesopores. The N_2 adsorption–desorption analysis (Figure 3C and D) manifested that the MSN and the EGCG@nHAp@MSN showed a type IV isotherm, which was indicative of the presence of mesopores. The former displayed the Type H1 hysteresis loop while the latter displayed a Type H3 hysteresis loop. The specific surface area and the pore volume decreased after the encapsulation of nHAp and EGCG (Table 1). The zeta potentials of nHAp@MSN, EGCG, and EGCG@nHAp@MSN were −10.9, −16.9, and −20.2 mV, respectively (Figure 3E–G).

Assessment of Dentin Permeability

The data of the dentin permeability derived from each time point are shown in Figure 4. Irrespective of the storage period (1 week or 1 month), significant main effects by group ($p < 0.001$), time point ($p < 0.001$), and group × time point interactions ($p < 0.001$) on the dentin permeability were noted from the two-factor repeated-measurements ANOVA. Irrespective of the storage period, the dentin permeability deceased significantly after the EGCG@nHAp@MSN treatment ($p < 0.001$). The Lp% value from this treatment group was significantly lower than values recorded in the two other groups ($p < 0.001$).

After the acid challenge (Figure 4A and C), regardless of 1 week or 1 month measurement, the dentin permeability in the control and the CPP–ACP groups increased significantly ($p < 0.001$), but no statistically significant increase was observed from the EGCG@nHAp@MSN treatment group ($p > 0.05$). Moreover, the Lp% value from this treatment group was the lowest of the three treatment groups ($p < 0.001$).

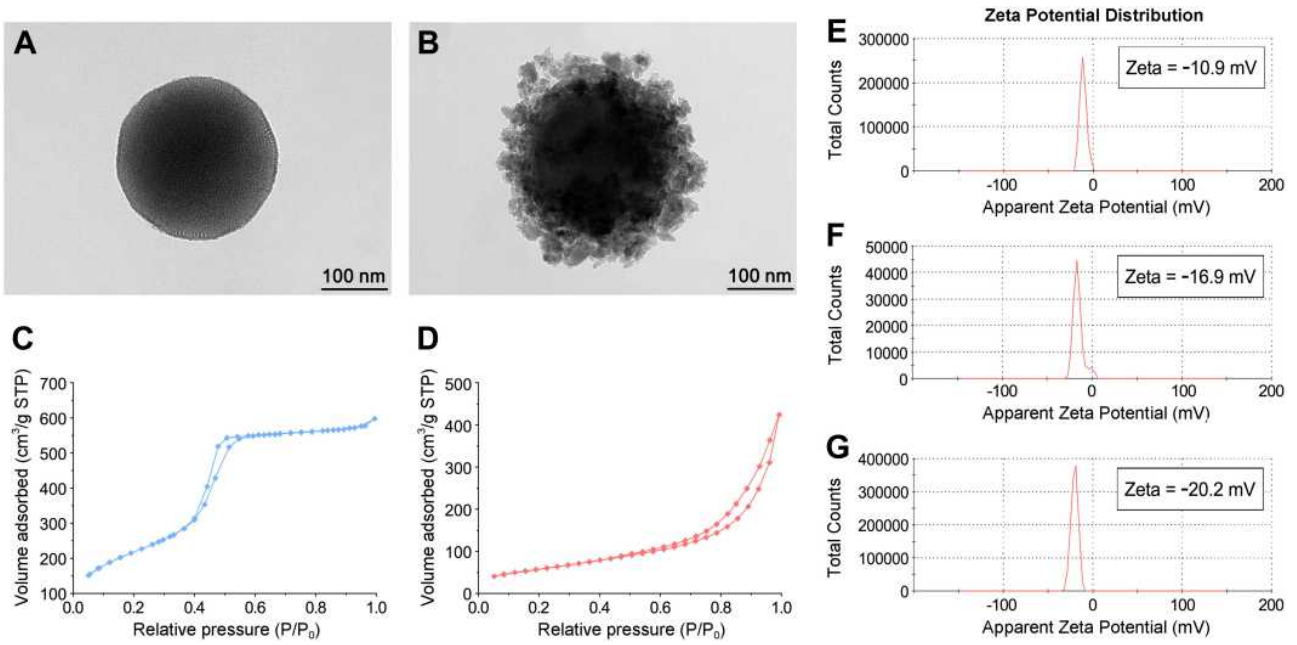

Figure 3 Ultrastructure and surface characteristics of MSN and EGCG@nHAp@MSN.
Notes: TEM images of (**A**) MSN and (**B**) EGCG@nHAp@MSN. Nitrogen adsorption–desorption isotherms of (**C**) MSN and (**D**) EGCG@nHAp@MSN. Zeta potentials of (**E**) nHAp@MSN, (**F**) EGCG, and (**G**) EGCG@nHAp@MSN.
Abbreviations: TEM, transmission electron microscopy; MSN, mesoporous silica nanoparticles; EGCG, epigallocatechin-3-gallate; EGCG@nHAp@MSN, epigallocatechin-3-gallate-encapsulated nanohydroxyapatite/mesoporous silica nanoparticles (mesoporous delivery system); nHAp@MSN, nanohydroxyapatite/mesoporous silica nanoparticles.

After the abrasion challenge (Figure 4B and D), regardless of 1 week or 1 month measurement, the dentin permeability in the CPP–ACP group increased ($p < 0.05$), but the two other groups did not experience statistically significant increases ($p > 0.05$). Furthermore, the lowest Lp% value of the three treatment groups was found in the EGCG@nHAp@MSN group ($p < 0.001$).

Tubule Occlusion Examination

The FESEM images of tubule occlusion after surface treatments are summarized in Figure 5. After 1 week of storage, open tubules with a smear-free layer were evident in the control group (group 1, Figure 5A1–A3). A portion of the sealed tubules with about 3 μm crystal infiltration could be seen in the CPP–ACP group (group 2, Figure 5B1–B3). Absolutely occluded tubules with 20 μm precipitate penetration were observed from the EGCG@nHAp@MSN group (group 3, Figure 5C1–C3). After 1 month of storage, group 1 showed all open tubules (Figure 5A4–A6). A small percentage of the blocked tubules with superficial crystal infiltration appeared in group 2 (Figure 5B4–B6). Completely obstructed tubules with approximately 18 μm precipitate penetration from the orifice were found in group 3 (Figure 5C4–C6). These precipitates were tightly integrated with internal tube walls.

Table 1 Nitrogen Adsorption Results

Samples	S_{BET} (m^2/g)	V_p (cm^3/g)	D_p (nm)
MSN	847.1	0.930	4.39
EGCG@nHAp@MSN	226.3	0.482	8.51

Abbreviations: S_{BET}, specific surface area; V_p, average pore volume; D_p, average pore diameter; MSN, mesoporous silica nanoparticles; EGCG@nHAp@MSN, epigallocatechin-3-gallate-encapsulated nanohydroxyapatite/mesoporous silica nanoparticles (mesoporous delivery system).

Acid Resistance Examination

The FESEM images after surface treatments, storage, and acid challenge are provided in Figure 6. After 1 week of storage and acid challenge, open tubules with enlarged diameters and a neat surface manifested in group 1 (Figure 6A1–A3). A majority of the open orifices were discovered with enlarged diameters and sporadic crystal infiltration in group 2 (Figure 6B1–B3). A large proportion of the tubules remained occluded, and 15 μm precipitate penetration from the orifice was observed in group 3 (Figure 6C1–C3). Although some orifices were slightly open, the underlying tubules were closely plugged by the

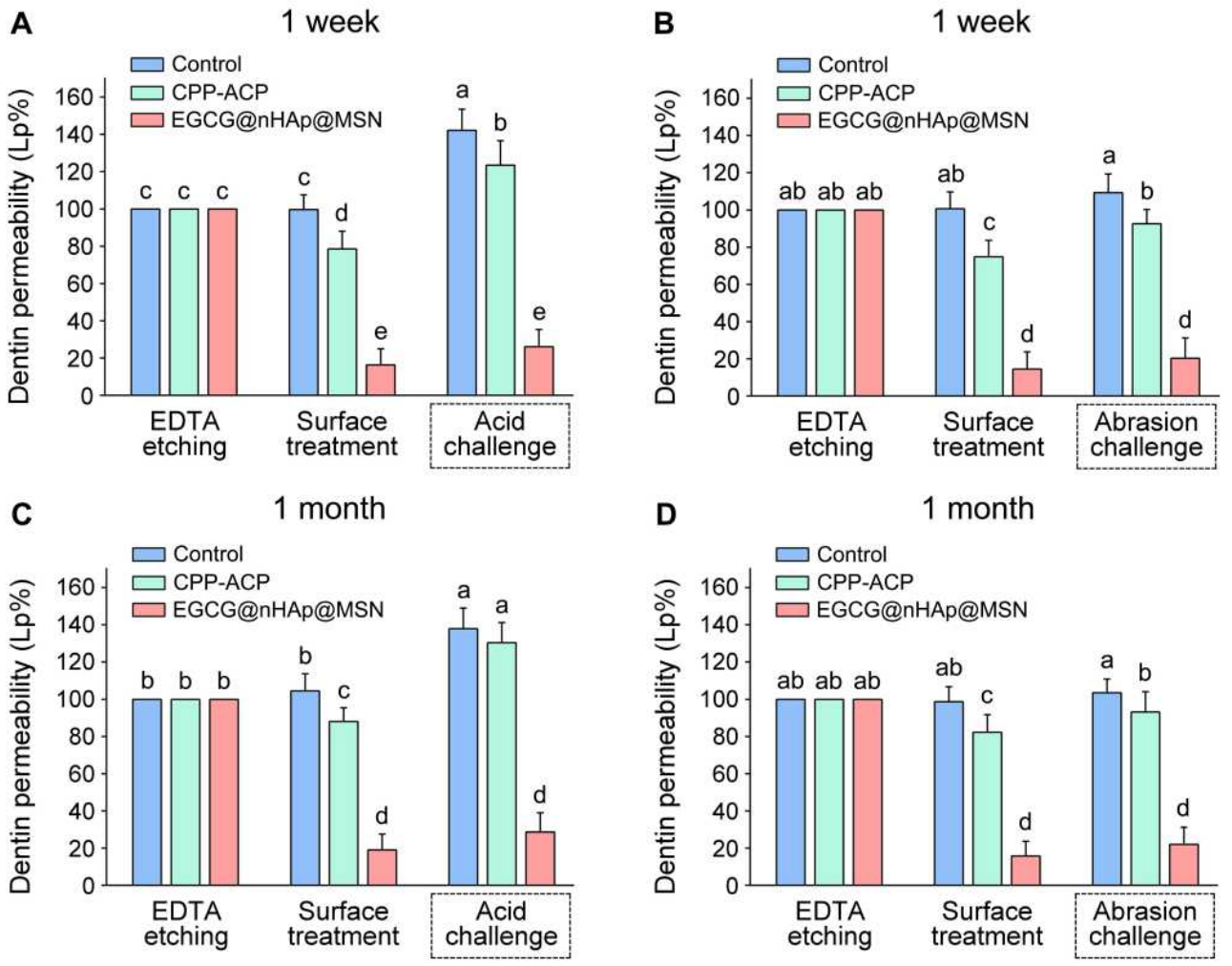

Figure 4 Dentin permeability values from each time point (subjected to EDTA etching, surface treatments, acid challenge, or abrasion challenge) for (**A** and **B**) 1 week or (**C** and **D**) 1 month of storage.

Notes: Data are represented as percentage (Lp%) and expressed as mean ± standard deviation. The maximum permeability (100%) was defined as Lp% that was obtained after EDTA etching. Groups with different letters (a–e) are significantly different ($p < 0.05$, n = 8).

Abbreviations: EDTA, ethylenediamine tetraacetic acid; Lp, hydraulic conductance.

precipitates. After 1 month of storage and acid challenge, tubules with enlarged diameters were all open in group 1 (Figure 6A4–A6). Almost all tubules with enlarged diameters were open in group 2 (Figure 6B4–B6). The vast majority of the tubules were still obstructed with 15 μm precipitate penetration from the orifice in group 3 (Figure 6C4–C6). These precipitates were well preserved inside the underlying tubules and membrane-like covering layers were formulated.

Abrasion Resistance Examination

The FESEM images after surface treatments, storage, and abrasion challenge are shown in Figure 7. After 1 week of storage and abrasion challenge, open tubules with remnant debris were found in group 1 (Figure 7A1–A3). A fraction of the sealed orifices was exhibited in group 2 (Figure 7B1–B3). Totally occluded tubules with a rough surface were observed in group 3 (Figure 7C1–C3). The precipitates of EGCG@nHAp@MSN were tightly integrated with internal tube walls with 15 μm penetration from the orifice. After 1 month of storage and abrasion challenge, all tubules were open with some debris in group 1 (Figure 7A4–A6). Scarcely any blocked tubules with a rough surface were found in group 2 (Figure 7B4–B6). Entirely obstructed tubules with approximately 10 μm precipitate penetration from the orifice remained in group 3 (Figure 7C4–C6).

CLSM and FESEM of Biofilm Inhibition

The *S. mutans* biofilm growth on dentin surfaces from three-dimensional overlay CLSM images is exhibited in

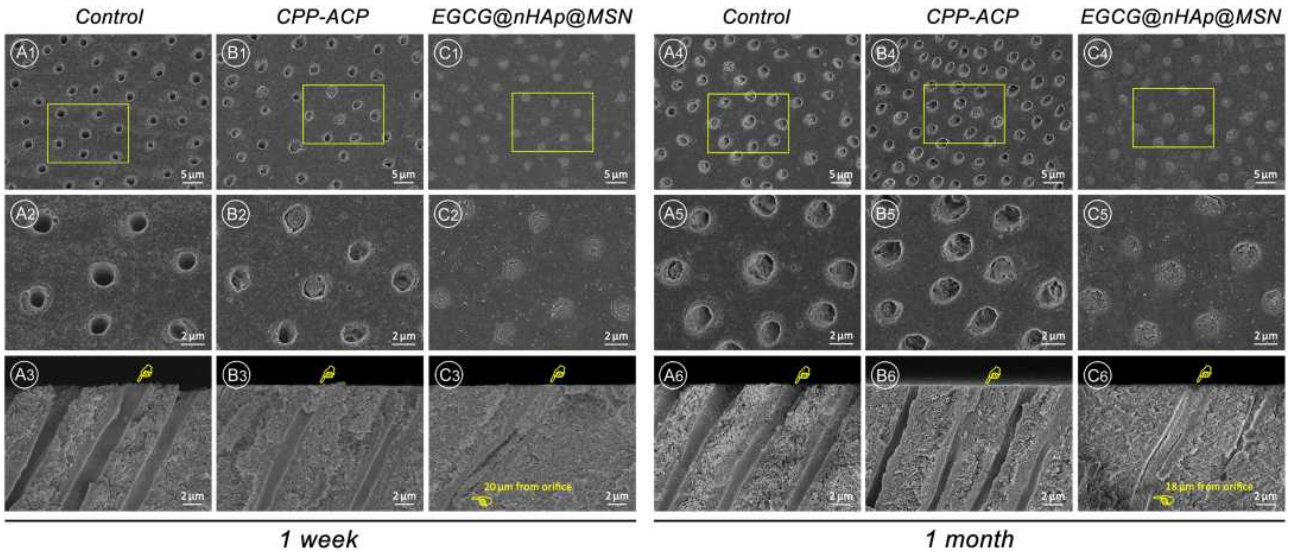

Figure 5 Tubule occlusion from FESEM cross- and longitudinal-section observation after surface treatments.
Notes: For 1 week of storage, apparent patent tubules with a smear-free layer in group 1 (control, **A1**–**A3**), partially blocked tubules in group 2 (CPP–ACP, **B1**–**B3**), and completely obstructed tubules with 20 μm precipitate penetration depth in group 3 (EGCG@nHAp@MSN, **C1**–**C3**) were discovered. For 1 month of storage, all patent tubules in group 1 (**A4**–**A6**), few sealed tubules with superficial crystal infiltration in group 2 (**B4**–**B6**), and absolutely occluded tubules with 18 μm penetration depth, in which precipitates were tightly integrated with internal tube walls, in group 3 (**C4**–**C6**) were captured. Images of (**A2**–**C2** and **A5**–**C5**) correspond to the high-magnification images of the yellow square region in (**A1**–**C1** and **A4**–**C4**). Pointers denote the dentinal tubules.
Abbreviations: FESEM, field-emission scanning electron microscopy; CPP–ACP, casein phosphopeptide-amorphous calcium phosphate; EGCG@nHAp@MSN, epigallocatechin-3-gallate-encapsulated nanohydroxyapatite/mesoporous silica nanoparticles (mesoporous delivery system).

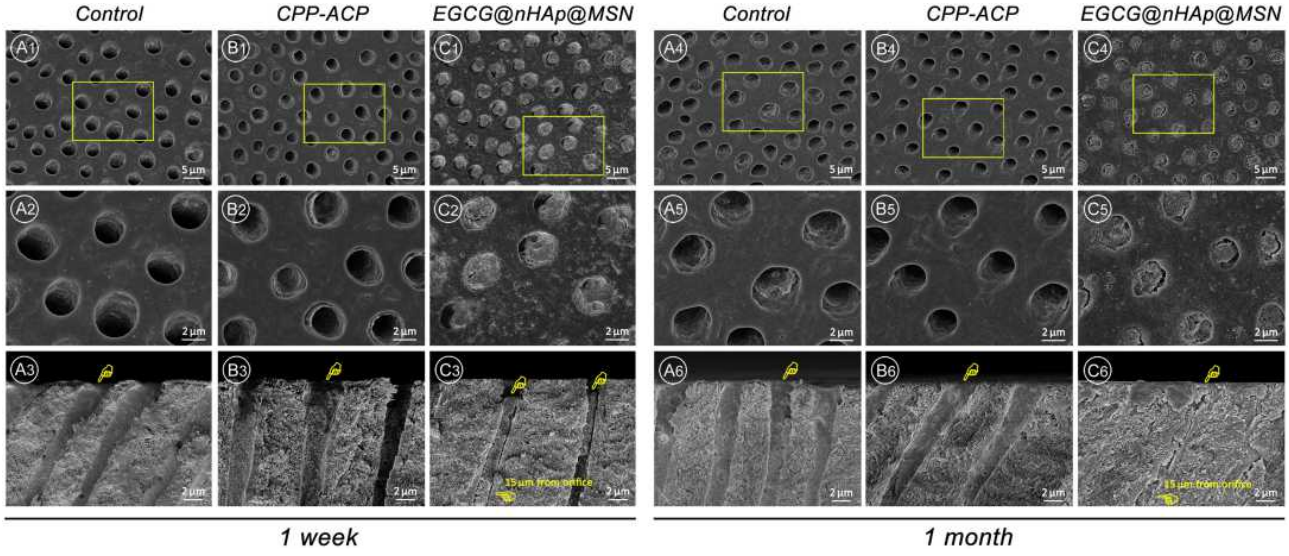

Figure 6 Tubule occlusion from FESEM cross- and longitudinal-section observation after surface treatments and storage and then subjected to acid challenge.
Notes: For 1 week of storage, expanded patent tubules in group 1 (control, **A1**–**A3**), a majority of expanded patent tubules with scattered crystal infiltration in group 2 (CPP–ACP, **B1**–**B3**), and a high percentage of obstructed tubules with 15 μm precipitate infiltration depth in group 3 (EGCG@nHAp@MSN, **C1**–**C3**) were discovered. For 1 month of storage, all expanded patent tubules in group 1 (**A4**–**A6**), almost all expanded patent tubules in group 2 (**B4**–**B6**), and the vast majority of occluded tubules with 15 μm infiltration depth, in which precipitates were well preserved inside the underlying tubule, in group 3 (**C4**–**C6**) were captured. Images of (**A2**–**C2** and **A5**–**C5**) correspond to the high-magnification images of the yellow square region in (**A1**–**C1** and **A4**–**C4**). Pointers denote the dentinal tubules.
Abbreviations: FESEM, field-emission scanning electron microscopy; CPP–ACP, casein phosphopeptide-amorphous calcium phosphate; EGCG@nHAp@MSN, epigallocatechin-3-gallate-encapsulated nanohydroxyapatite/mesoporous silica nanoparticles (mesoporous delivery system).

Figure 8A1–C1 and A2–C2. Live/dead bacteria in each layer from corresponding CLSM images were represented by biomass distribution (Figure 8A1–C1 and A2–C2). After 1 week of storage, the EGCG@nHAp@MSN group revealed significantly fewer live/dead bacteria compared with the two other groups (Figure 8A1–C1). Measurements of total biomass in the EGCG@nHAp@MSN group manifested

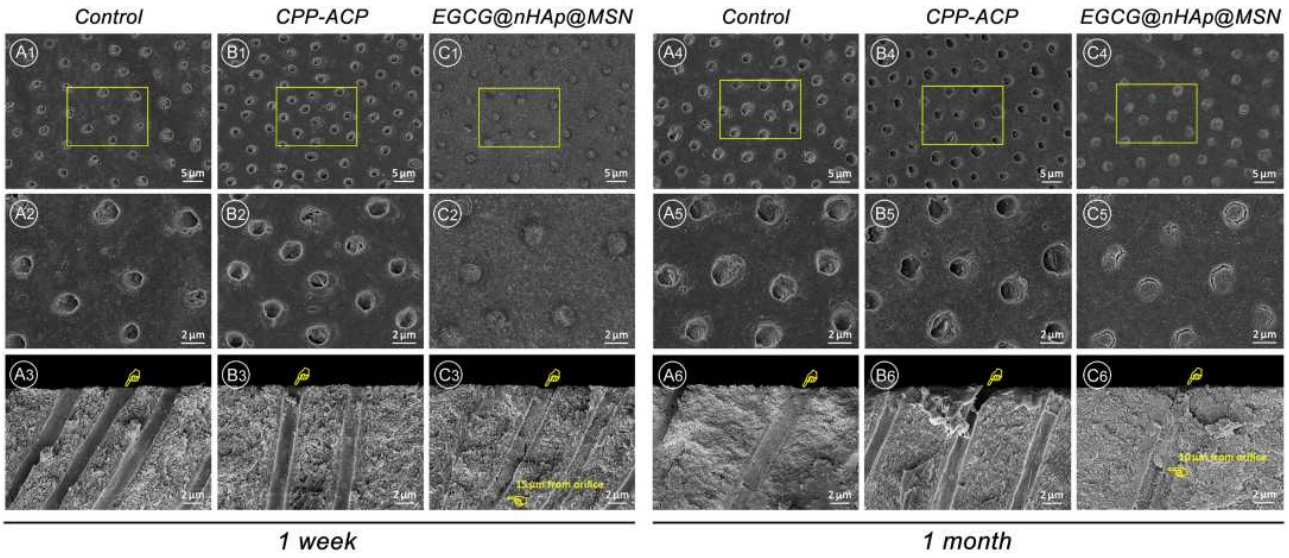

Figure 7 Tubule occlusion from FESEM cross- and longitudinal-section observation after surface treatments and storage and then subjected to abrasion challenge.
Notes: For 1 week of storage, for 1 week of storage, distinct patent tubules with surface debris in group 1 (Control, **A1**–**A3**), a small quantity of the blocked tubules in group 2 (CPP–ACP, **B1**–**B3**), and entirely obstructed tubules with 15 μm infiltration depth, in which precipitates were tightly combined with internal tube walls, in group 3 (EGCG@nHAp@MSN, **C1**–**C3**) were discovered. For 1 month of storage, all patent tubules with few debris in group 1 (**A4**–**A6**), barely any blocked tubules with a rough surface in group 2 (**B4**–**B6**), and totally occluded tubules with the well-maintained precipitate infiltration depth of 10 μm in group 3 (**C4**–**C6**) were captured. Images of (**A2**–**C2** and **A5**–**C5)** correspond to the high-magnification images of the yellow square region in (**A1**–**C1** and **A4**–**C4)**. Pointers denote the dentinal tubules.
Abbreviations: FESEM, field-emission scanning electron microscopy; CPP–ACP, casein phosphopeptide-amorphous calcium phosphate; EGCG@nHAp@MSN, epigallocatechin-3-gallate-encapsulated nanohydroxyapatite/mesoporous silica nanoparticles (mesoporous delivery system).

a significant decrease at the 10th layer (20 μm), whereas the two other groups exhibited an upward trend. After 1 month of storage, despite an increase in the amounts of live/dead bacteria in all three groups compared with quantities after 1 week of storage, the EGCG@nHAp@MSN group still revealed significantly fewer live/dead bacteria compared with the two other groups (Figure 8A2–C2). The total biomass in the EGCG@nHAp@MSN group significantly decreased at the 10th layer, whereas the two other groups displayed an apparent upward trend.

The *S. mutans* adherence and biofilm growth on dentin surfaces from representative FESEM images are displayed in Figure 8A3–C3 and A4–C4. Compared with the control group, the CPP–ACP group revealed relatively low levels of bacteria adhesion after 1 week of storage. The EGCG@nHAp@MSN group showed completely obstructed orifices and significantly fewer bacteria among the three groups (Figure 8A3–C3 and A3–C3). After 1 month of storage, a thick and extensive biofilm was formed in both the control and the CPP–ACP groups. Significantly less biofilm was formed in the EGCG@nHAp@MSN group with blocked orifices compared with the two other groups (Figure 8A4–C4 and A4–C4).

CFU and MTT of Biofilm Inhibition

The inhibitory effects on the *S. mutans* colony reproduction and the metabolic activities from the CFU and the MTT assays after surface treatments are depicted in Figure 9. Regardless of the CFU or the MTT data, significant differences by group ($p < 0.001$), storage time ($p < 0.001$), and group × storage time interactions ($p < 0.001$) were noted from the two-factor ANOVA. After 1 week of storage, there was no statistical difference between the control and the CPP–ACP groups ($p > 0.05$), irrespective of the CFU or the MTT data. Meanwhile, the EGCG@nHAp@MSN group exhibited the fewest colonies (Figure 9A) and the lowest metabolic activity (Figure 9B) of the three groups ($p < 0.05$). After 1 month of storage, no statistical difference between the control and the CPP–ACP groups was noted ($p > 0.05$), irrespective of the CFU or the MTT data. The CFU and the MTT values in the EGCG@nHAp@MSN group represented the fewest colonies and the lowest metabolic activity of the three groups ($p < 0.05$).

Cytotoxicity

Figure 9C manifests the relative cell viability of HDPCs cultured with EGCG@nHAp@MSN (0, 250, 500, and 1000 μg/mL) for 1, 3, and 7 days. After 1 or 3 days of

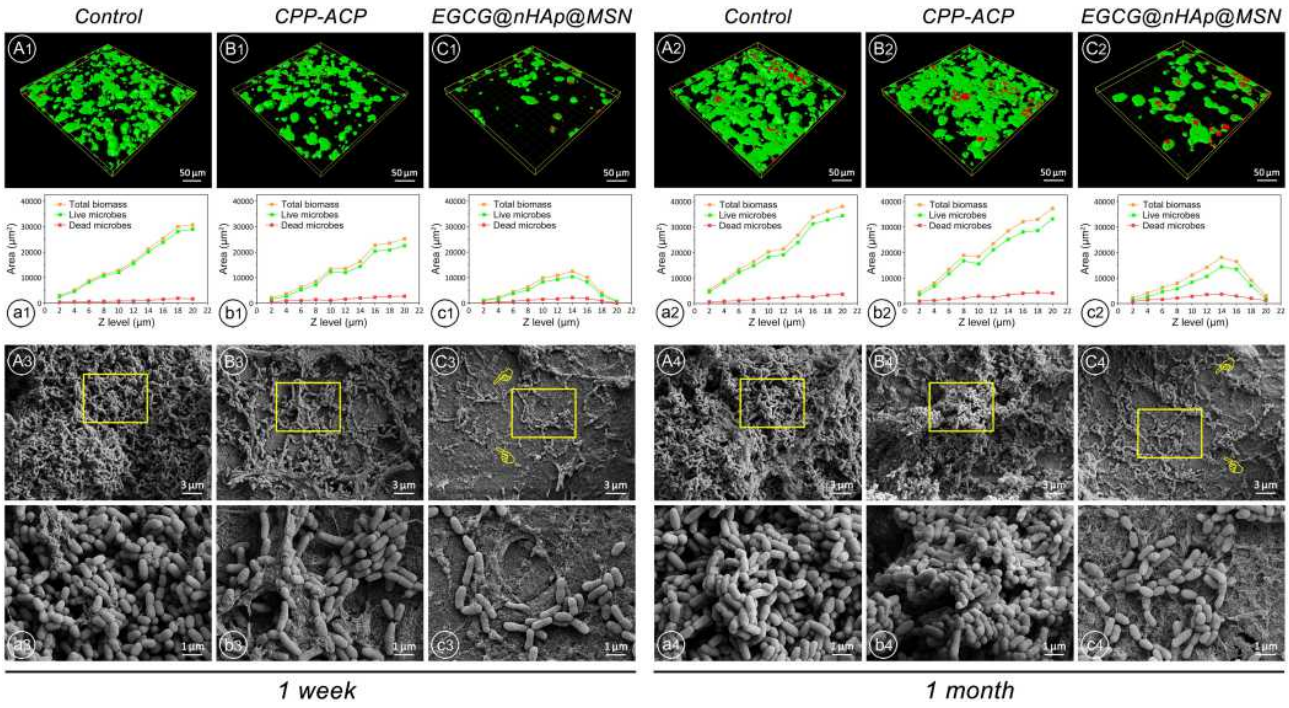

Figure 8 *S. mutans* biofilm grown on dentin surfaces from CLSM and FESEM images.
Notes: (**A1**–**C1** and **A2**–**C2**) Biofilm formation from representative z-stacked 3D CLSM images of each group. Live/dead (green/red) bacteria of each layer at the z-step for each group are expressed by biomass distribution (**A1**–**C1** and **A2**–**C2**) plotted below the corresponding CLSM image. (**A3**–**C3** and **A4**–**C4**) Biofilm adherence and grown from representative FESEM images of each group. Images of (**A3**–**C3** and **A4**–**C4**) correspond to the high-magnification images of the yellow square region in (**A3**–**C3** and **A4**–**C4**). Pointers denote obstructed orifices by EGCG@nHAp@MSN.
Abbreviations: *S. mutans, Streptococcus mutans*; CLSM, confocal laser scanning microscopy; FESEM, field-emission scanning electron microscopy; EGCG@nHAp@MSN, epigallocatechin-3-gallate-encapsulated nanohydroxyapatite/mesoporous silica nanoparticles (mesoporous delivery system).

incubation, no significant difference in the relative cell viability of HDPCs was noted among the concentration groups ($p > 0.05$), and the cell viability at all concentrations was higher than 90%. Moreover, even after 7 days of incubation, the cell viability of HDPCs exposed to EGCG@nHAp@MSN at the highest concentration (1000 μg/mL) still exceeded 85%.

Profiles of EGCG, Ca, and P Release

The in vitro cumulative EGCG, Ca, and P release of the mesoporous delivery system is shown in Figure 10. A trend for a relatively rapid release in the first 7 days and a sustained release to the 30th day were observed for EGCG (Figure 10A), and nearly 70% of EGCG was released after 30 days of measurement on the basis of its standard curve ($y = 0.0036x + 0.0168$; $R^2 = 0.9994$). Meanwhile, a stable release of Ca and P ions until the 30th day was evident in Figure 10B.

Discussion

In this study, the feasibility of a mesoporous delivery system to serve as a dentin surface biobarrier and its stability to protect the exposed dentin are investigated. Results demonstrate that the mesoporous delivery system effectively occludes dentinal tubules with acid and abrasion resistance and decreases dentin permeability for up to 1 month. These findings suggest that prolonged sealing stability is achieved. Thus, the first and the second hypotheses are accepted.

Human oral cavity is a relatively complicated environment. After the tooth preparation during the process of the indirect restoration, the exposure of dentin may be susceptible to post-operative sensitivity and face with several adverse challenges, including the acid, abrasion, and cariogenic bacteria attack.[13,19,20] It is actually not associated with specific oral diseases but is linked to different challenges in oral environment. Given the tubular structure and the low mineralization of dentin,[4] an effective surface biobarrier after the enamel destruction can play a significant role in combating adverse challenges and protecting internal dentin and pulp tissue. On account of the superior characteristics of EGCG, nHAp, and MSN, the mesoporous silica-based delivery system (EGCG@nHAp@MSN) is highly suitable for establishing

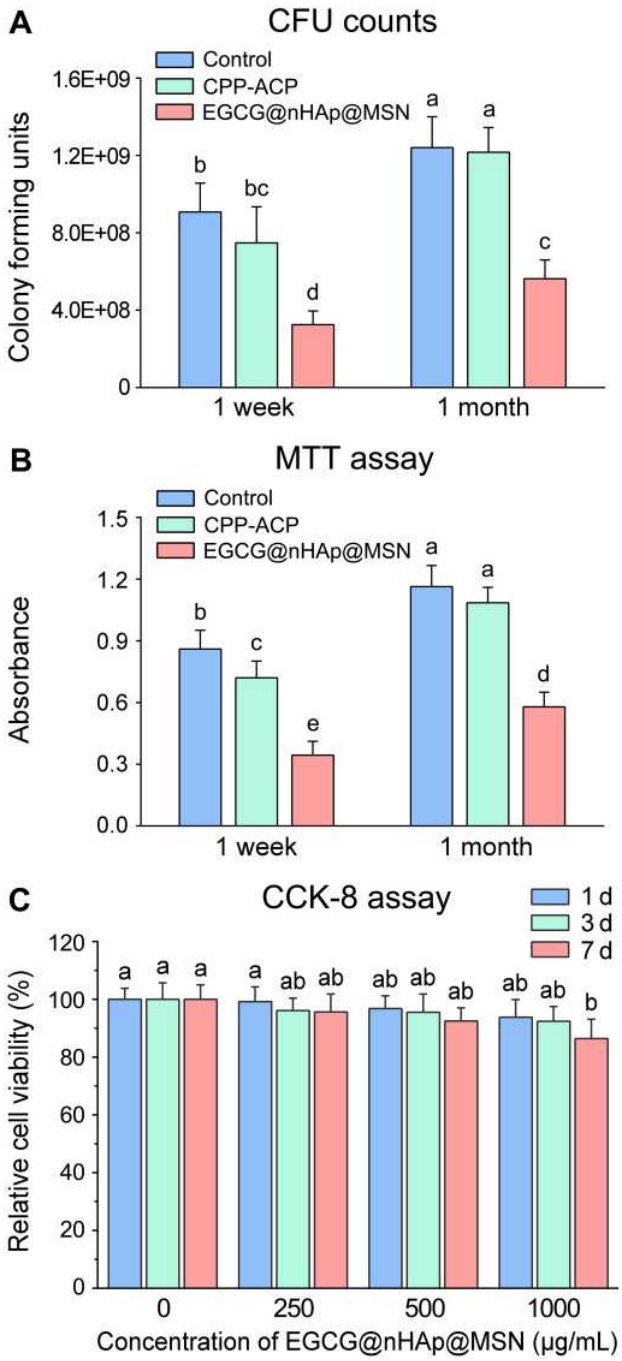

Figure 9 *S. mutans* biofilm grown on dentin surfaces from CFU counts and MTT assay and cytotoxicity of EGCG@nHAp@MSN from CCK-8 assay.

Notes: (**A**) Biofilm formation from CFU counts of each group after 1 week or 1 month of storage. CFU data are represented as mean ± standard deviation. Groups with different letters (a–d) are significantly different ($p < 0.05$, n = 9). (**B**) Biofilm formation from MTT assay of each group after 1 week or 1 month of storage. MTT data are represented as mean ± standard deviation. Groups with different letters (a–e) are significantly different ($p < 0.05$, n = 12). (**C**) Relative cell viability of HDPCs exposed to different concentrations of EGCG@nHAp@MSN after 1, 3, and 7 days of incubation. CCK-8 data are expressed as mean ± standard deviation. Statistical analysis against the control (0 μg/mL) was performed. Groups with different letters (a and b) are significantly different ($p < 0.05$, n = 6).

Abbreviations: *S. mutans*, *Streptococcus mutans*; CFU, colony-forming unit; MTT, 3-(4,5-dimethylthiazol-2-yl)-2,5-diphenyltetrazolium bromide; EGCG@nHAp@MSN, epigallocatechin-3-gallate-encapsulated nanohydroxyapatite/mesoporous silica nanoparticles (mesoporous delivery system); CCK-8, Cell Counting Kit-8; HDPCs, human dental pulp cells.

such a biobarrier. A homogeneous precipitation technique is used in the present study to fabricate the mesoporous delivery system, and TEM images of the system indicate a well-maintained framework and successful incorporation of EGCG and nHAp into MSN (Figure 3B). The N_2 adsorption–desorption analysis reveals that the specific

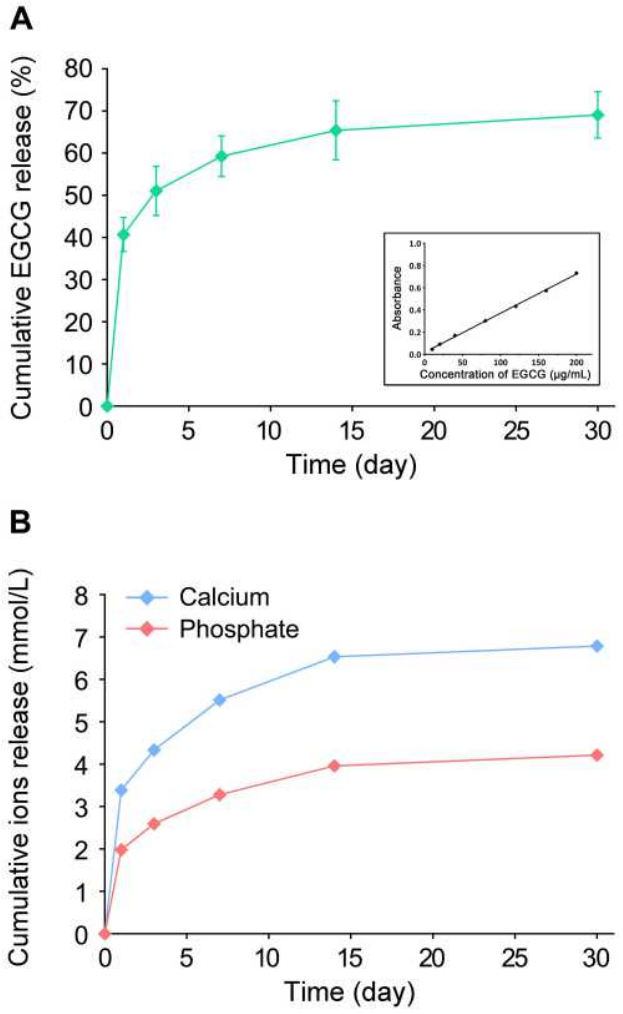

Figure 10 In vitro cumulative release of (**A**) EGCG and (**B**) Ca and P of EGCG@nHAp@MSN in sterile deionized water for 30 days at 37 °C.
Abbreviations: EGCG, epigallocatechin-3-gallate; EGCG@nHAp@MSN, epigallocatechin-3-gallate-encapsulated nanohydroxyapatite/mesoporous silica nanoparticles (mesoporous delivery system).

surface area and the pore volume decrease after the encapsulation of nHAp and EGCG (Table 1), but the EGCG@nHAp@MSN still exhibits a type IV isotherm, which is indicative of the presence of mesopores (Figure 3D). Theoretically, the high surface area, pore volume, and channel structure make the effective encapsulation of drug molecules within the MSN pores feasible; the reason may be derived from the drug interaction with the pore walls via van der Waals interactions, electrostatic binding, hydrogen bonding, and covalent bonding.[36–38] Thus, the electrostatic binding may not be the dominant mechanism for the adsorption of EGCG by the nHAp@MSN in accordance with the zeta potential results (Figure 3E–G). In vitro release profiles indicate that mesoporous silica can act as a reservoir and a carrier to deliver sustainable supplies of calcium and phosphate ions and EGCG molecules (Figure 10), suggesting the potential to realize a durable system for managing the exposed dentin.

According to the hydrodynamic theory, the effective occlusion of exposed dentinal tubules is a reliable regimen and a prerequisite for decreasing dentin permeability and avoiding irritants invasion to treat related dental diseases.[39] The consistent outcomes with respect to the dentin permeability (Figure 4) and FESEM inspections (Figure 5) support the hydrodynamic theory and indicate that the mesoporous delivery system can reduce the dentin permeability and obstruct dentinal tubules efficiently for 1 month. Several mechanisms may contribute to this phenomenon. Initially, the average size of the EGCG@nHAp@MSN (approximately 300 nm) is far smaller than the diameter of the tubules. Polishing using a slurry of materials facilitates the ability to permeate the tubules deeply.[40,41] What's more, uniformly loaded nHAp on MSN can complement and occupy the gaps between each silica sphere inside the tubules and readily bind to other atoms and dentin matrix due to the high surface energy associated with large atomic numbers.[42] These characteristics endowed the EGCG@nHAp@MSN with favorable capacity to block the orifices of the tubules tightly and integrate with interior tubular walls. Besides, the local supersaturation of sustained released calcium and phosphate ions likely promotes the mineral deposition inside the tubules, not merely on the dentin surface.[43,44]

An oral environment for the routine acid challenge is simulated by utilizing the citric acid solution with the concentration of 6% (w/v) to assess the acid resistance since the main acidic ingredient in dietary soft drinks or fruit juices is citric acid.[19,45] The results for dentin permeability (Figure 4) and FESEM (Figure 6) confirm the efficacy of the mesoporous delivery system with respect to acid resistance for 1 month. This finding can be attributed to the outstanding aciduric stability of mesoporous silica.[46] Although loose deposits around the orifices are dissolved to some extent, underlying precipitates are well retained because such stability protects the precipitates from erosional forces and because of the solid integration between the EGCG@nHAp@MSN and tubular internal walls before the acid challenge. Additionally, the nHAp holds the potential to extract Ca and P for the remineralization along the tubules and the creation of covering layers on the dentin surface,[47] and the degradation of dentin collagen induced by matrix metalloproteinases can be inactivated by EGCG to tolerate erosion.[48] The tubular

diameter and the dentin permeability in the control group increase after the acid challenge because the peritubular dentin is vulnerable to acidic attacks, as previously reported.[49,50] As a milk protein derivative, the CPP–ACP complex can remineralize the dentin to block dentinal tubules.[51] Increased dentin permeability after the acid challenge is observed in the CPP–ACP group, denoting its incompetence in maintaining relatively lasting tubule-sealing effects, and acid erosion cannot be countered due to insufficient remineralization.[52]

The Abrasion resistance is also investigated in this study as mechanical brushing or abrasion readily reopens obstructed tubules and removes covering layers.[19,53] The results of the dentin permeability (Figure 4) and the FESEM examination (Figure 7) highlight the efficiency of the mesoporous delivery system with regard to the abrasion resistance after 1 month. Probable mechanisms should be illustrated as follows. On the one hand, the satisfactory mechanical strength from mesoporous silica undoubtedly contributes to the enhancement of the anti-abrasion action.[54] On the other hand, the likelihood of being brushed away can be minimized by the compact filling of EGCG@nHAp@MSN precipitates inside the tubules, and the involvement of nHAp supplements the remineralization effect.[55] By contrast, the loose and the inadequate occlusion of CPP–ACP materials results in a large proportion of patent tubules and increased permeability, which represented unendurable abrasion resistance.

Although the efficacy of different desensitizing approaches on the occlusion of dentinal tubules is extensively investigated, these therapies are not generally associated with the effective integration of antibiofilm and tubule-sealing abilities or long-lasting action. Inferior blocked tubules that remain provide available pathways for bacterial invasion and aggregation, thereby producing acid compounds by metabolizing carbohydrates, causing dentin demineralization and caries, and influencing the stability of already occluded tubules.[56] The conundrums regarding the adherence and the growth of cariogenic bacteria and biofilms on exposed dentin surfaces should be addressed during the process of the indirect restoration. CLSM, FESEM, CFU, and MTT analyses (Figures 8 and 9) verify that the mesoporous delivery system effectively inhibits the *S. mutans* adherence and the biofilm formation on dentin surfaces for up to 1 month. These findings suggest that prolonged antibiofilm stability is obtained. Thus, the third hypothesis is accepted.

Considering the components of EGCG@nHAp@MSN, several points contribute to the inhibitory function. First, the continuous release of EGCG from the mesoporous delivery system unfolds over 30 days in vitro (Figure 10A), suggesting an essential role in providing the sustainable suppression of the biofilm formation for 1 month. Second, the attachment of *S.mutans* on the dentin matrix can be interfered through restraining glucosyltransferase B, C, and D gene expression by EGCG,[57] and the cariogenicity of *S.mutans* can also be suppressed through controlling its acidic production and virulence factors, such as lactate dehydrogenase.[58] Third, numerous nanopores in the mesoporous silica provide a favorable reservoir to absorb EGCG molecules and Ca and P ions, enabling a stable release during 30 days (Figure 10). This phenomenon may endow the acid-etched dentin with considerable remineralization capability and protect the exposed dentin collagen by neutralizing acids for combating tooth decay.[59,60]

Given that nanoparticles may infiltrate into the pulp cavity via the dentinal tubules and interact with the vital pulp tissue, the biocompatibility should be considered to assess the safety of synthetic biomaterials. The cytotoxicity of EGCG@nHAp@MSN on the proliferation of HDPCs is conducted using the CCK-8 assay. This assay is accomplished by culturing the pulp cells with EGCG@nHAp@MSN (0, 250, 500, and 1000 μg/mL) for 1, 3, and 7 days (Figure 9C). After 1 or 3 days of incubation, the relative cell viability at all concentrations is higher than 90%. What's more, the viability of HDPCs exposed to EGCG@nHAp@MSN at the highest concentration (1000 μg/mL) still exceeds 85% even after 7 days of incubation. Hence, the mesoporous delivery system is proven to possess relatively low cytotoxicity to pulp cells and may be suitable for in vivo application.

Since this study aims to determine the stability of the mesoporous delivery system on the tubule occlusion and the biofilm inhibition, a material that can provide tubule-occluding and anti-biofilm effects could serve as a positive control to be fairly compared with the EGCG@nHAp@MSN. Thus, the commercial available CPP-ACP-contained paste is selected appropriately as the positive control because its tubule-occluding and anti-biofilm efficacy has been reported previously.[19,61–63] Although a paste form, a slurry of the CPP-ACP-contained paste can be achieved during the polishing procedure because dentin is a moist substrate. The comparison between EGCG@nHAp@MSN and CPP-ACP would be more likely to highlight the practical clinical value. In

addition, it should be noteworthy that the discs are stored in artificial saliva for dentin permeability assessment and tubule occlusion examination to simulate clinical conditions better. Whereas sterile deionized water is used for antibiofilm experiments because the cultivation of cariogenic bacteria has relatively strict requirements, and the antibiofilm ability may be interfered by different factors in other storage media. A series of previous research has used sterile deionized water as the storage medium to evaluate the antibiofilm activity of the synthetic dental materials.[64–66] In line with the reported methods, our experiments are carried out by using sterile deionized water. As for the measurement of EGCG, Ca, and P release, sterile deionized water is utilized to avoid the influence of Ca and P ions existing in artificial saliva, simulated body fluid (SBF), or PBS.

Based on these results, the mesoporous delivery system can continuously release EGCG, Ca, and P; efficiently occlude dentinal tubules with acid and abrasion resistance; reduce the dentin permeability; and inhibit the *S.mutans* adhesion and biofilm formation for up to 1 month for the first time. These findings confirm that the mesoporous delivery system can serve as an effective surface biobarrier and provide desirable sealing and antibiofilm stability to protect the exposed dentin against external challenges. This work bridges the gap between the clinical practice and the versatile biomaterial research and offers a promising framework for overcoming the dentin hypersensitivity and caries after the enamel damage. Further studies are needed to explore the effects of the engineered biobarrier on the bond stability at adhesive–dentin interfaces and the potential application in clinical dentistry.

Conclusion

This study aimed at evaluating the stability of the dentin surface biobarrier consisting of mesoporous silica-based EGCG/nHAp delivery system on the tubule occlusion and the *S.mutans* biofilm inhibition. The engineered surface biobarrier persistently occluded dentinal tubules with acid and abrasion resistance and inhibited the *S. mutans* biofilm formation for up to 1 month. This biobarrier provided prolonged stability for protecting the underlying dentin to combat adverse challenges in oral environments. Therefore, the establishment of the dentin surface biobarrier consisting of mesoporous delivery system suggested promising progress toward the prevention and the management of dentin hypersensitivity and caries after the enamel loss during the process of the indirect restoration.

Acknowledgments

This work was supported by the National Natural Science Foundation of China (grant numbers 81901043, 81970918, and 81701012).

Disclosure

The authors report no conflicts of interest in this work.

References

1. Shao C, Jin B, Mu Z, et al. Repair of tooth enamel by a biomimetic mineralization frontier ensuring epitaxial growth. *Sci Adv*. 2019;5(8):eaaw9569. doi:10.1126/sciadv.aaw9569
2. Lawn BR, Lee JJW, Chai H. Teeth: among nature's most durable biocomposites. *Annu Rev Mat Res*. 2010;40(1):55–75. doi:10.1146/annurev-matsci-070909-104537
3. An B, Wang R, Zhang D. Role of crystal arrangement on the mechanical performance of enamel. *Acta Biomater*. 2012;8(10):3784–3793. doi:10.1016/j.actbio.2012.06.026
4. Chiang YC, Lin HP, Chang HH, et al. A mesoporous silica biomaterial for dental biomimetic crystallization. *ACS Nano*. 2014;8(12):12502–12513. doi:10.1021/nn5053487
5. Palmer LC, Newcomb CJ, Kaltz SR, Spoerke ED, Stupp SI. Biomimetic systems for hydroxyapatite mineralization inspired by bone and enamel. *Chem Rev*. 2008;108(11):4754–4783. doi:10.1021/cr8004422
6. van den Breemer C, Gresnigt M, Özcan M, Kerdijk W, Cune MS. Prospective randomized clinical trial on the survival of lithium disilicate posterior partial crowns bonded using immediate or delayed dentin sealing: short-term results on tooth sensitivity and patient satisfaction. *Oper Dent*. 2019;44(5):E212–E222. doi:10.2341/18-047-C
7. Farias D, Walter R, Swift EJ. Critic appraisal. postoperative sensitivity with indirect restorations. *J Esthet Restor Dent*. 2014;26(3):208–213. doi:10.1111/jerd.12103
8. Murata T, Maseki T, Nara Y. Effect of immediate dentin sealing applications on bonding of CAD/CAM ceramic onlay restoration. *Dent Mater J*. 2018;37(6):928–939. doi:10.4012/dmj.2017-377
9. Magne P. Immediate dentin sealing: a fundamental procedure for indirect bonded restorations. *J Esthet Restor Dent*. 2005;17(3):144–-54; discussion155. doi:10.1111/j.1708-8240.2005.tb00103.x
10. Bekes K, Hirsch C. What is known about the influence of dentine hypersensitivity on oral health-related quality of life? *Clin Oral Investig*. 2013;17(1):S45–S51. doi:10.1007/s00784-012-0888-9
11. Pitts NB, Zero DT, Marsh PD, et al. Dental caries. *Nat Rev Dis Primers*. 2017;3(1):17030. doi:10.1038/nrdp.2017.30
12. West NX, Seong J, Davies M. Management of dentine hypersensitivity: efficacy of professionally and self-administered agents. *J Clin Periodontol*. 2015;42:S256–S302. doi:10.1111/jcpe.12336
13. Takahashi N, Nyvad B. Ecological hypothesis of dentin and root caries. *Caries Res*. 2016;50(4):422–431. doi:10.1159/000447309
14. Hahn CL, Liewehr FR. Relationships between caries bacteria, host responses, and clinical signs and symptoms of pulpitis. *J Endod*. 2007;33(3):213–219. doi:10.1016/j.joen.2006.11.008
15. Brannstrom M. Dentin sensitivity and aspiration of odontoblasts. *J Am Dent Assoc*. 1963;66(3):366–370. doi:10.14219/jada.archive.1963.0104

16. Rusin RP, Agee K, Suchko M, Pashley DH. Effect of a new desensitizing material on human dentin permeability. *Dent Mater*. 2010;26(6):600–607. doi:10.1016/j.dental.2010.02.010
17. Marto CM, Baptista Paula A, Nunes T, et al. Evaluation of the efficacy of dentin hypersensitivity treatments-a systematic review and follow-up analysis. *J Oral Rehabil*. 2019;46(10):952–990. doi:10.1111/joor.12842
18. Qanungo A, Aras MA, Chitre V, Mysore A, Amin B, Daswani SR. Immediate dentin sealing for indirect bonded restorations. *J Prosthodont Res*. 2016;60(4):240–249. doi:10.1016/j.jpor.2016.04.001
19. Wang Z, Ma X, Jiang T, Wang Y, Feng Y, Li R. The dentin tubule occlusion effects of desensitizing agents and the stability against acids and brushing challenges. *Am J Dent*. 2015;28(3):128–132.
20. João-Souza SH, Machado AC, Lopes RM, Zezell DM, Scaramucci T, Aranha ACC. Effectiveness and acid/tooth brushing resistance of in-office desensitizing treatments-a hydraulic conductance study. *Arch Oral Biol*. 2018;96:130–136. doi:10.1016/j.archoralbio.2018.09.004
21. Wang YY, Chatzistavrou X, Faulk D, et al. Biological and bactericidal properties of Ag-doped bioactive glass in a natural extracellular matrix hydrogel with potential application in dentistry. *Eur Cell Mater*. 2015;29:342–355. doi:10.22203/eCM.v029a26
22. Yang Y, Shen Y, Wang Z, et al. Evaluation of the susceptibility of multispecies biofilms in dentinal tubules to disinfecting solutions. *J Endod*. 2016;42(8):1246–1250. doi:10.1016/j.joen.2016.05.011
23. Xu YT, Wu Q, Chen YM, Smales RJ, Shi SY, Wang MT. Antimicrobial effects of a bioactive glass combined with fluoride or triclosan on streptococcus mutans biofilm. *Arch Oral Biol*. 2015;60(7):1059–1065. doi:10.1016/j.archoralbio.2015.03.007
24. Orchardson R, Gillam DG. Managing dentin hypersensitivity. *J Am Dent Assoc*. 2006;137(7):990–998. doi:10.14219/jada.archive.2006.0321
25. Yamagishi K, Onuma K, Suzuki T, et al. Materials chemistry: a synthetic enamel for rapid tooth repair. *Nature*. 2005;433(7028):819. doi:10.1038/433819a
26. Yu HH, Zhang L, Yu F, Li F, Liu ZY, Chen JH. Epigallocatechin-3-gallate and epigallocatechin-3-O-(3-O-methyl)-gallate enhance the bonding stability of an etch-and-rinse adhesive to dentin. *Materials*. 2017;10(2):183. doi:10.3390/ma10020183
27. Nguyen TL, Choi Y, Kim J. Mesoporous silica as a versatile platform for cancer immunotherapy. *Adv Mater*. 2019;31(34):e1803953. doi:10.1002/adma.201803953
28. Ni D, Jiang D, Ehlerding EB, Huang P, Cai W. Radiolabeling silica-based nanoparticles via coordination chemistry: basic principles, strategies, and applications. *Acc Chem Res*. 2018;51(3):778–788. doi:10.1021/acs.accounts.7b00635
29. Yu J, Yang H, Li K, Ren H, Lei J, Huang C. Development of epigallocatechin-3-gallate-encapsulated nanohydroxyapatite/mesoporous silica for therapeutic management of dentin surface. *ACS Appl Mater Interfaces*. 2017;9(31):25796–25807. doi:10.1021/acsami.7b06597
30. Hao X, Hu X, Zhang C, et al. Hybrid mesoporous silica-based drug carrier nanostructures with improved degradability by hydroxyapatite. *ACS Nano*. 2015;9(10):9614–9625. doi:10.1021/nn507485j
31. Wang Z, Sa Y, Sauro S, et al. Effect of desensitising toothpastes on dentinal tubule occlusion: a dentine permeability measurement and sem in vitro study. *J Dent*. 2010;38(5):400–410. doi:10.1016/j.jdent.2010.01.007
32. Islam MS, Hiraishi N, Nassar M, Yiu C, Otsuki M, Tagami J. Effect of hesperidin incorporation into a self-etching primer on durability of dentin bond. *Dent Mater*. 2014;30(11):1205–1212. doi:10.1016/j.dental.2014.08.371
33. Yu J, Zhang W, Li Y, et al. Synthesis, characterization, antimicrobial activity and mechanism of a novel hydroxyapatite whisker/nano zinc oxide biomaterial. *Biomed Mater*. 2014;10(1):015001. doi:10.1088/1748-6041/10/1/015001
34. Gong SQ, Epasinghe DJ, Zhou B, et al. Effect of water-aging on the antimicrobial activities of an ormosil-containing orthodontic acrylic resin. *Acta Biomater*. 2013;9(6):6964–6973. doi:10.1016/j.actbio.2013.02.031
35. Yang HY, Niu LN, Sun JL, et al. Biodegradable mesoporous delivery system for biomineralization precursors. *Int J Nanomedicine*. 2017;12:839–854. doi:10.2147/IJN.S128792
36. Butler KS, Durfee PN, Theron C, et al. Protocells: modular mesoporous silica nanoparticle-supported lipid bilayers for drug delivery. *Small*. 2016;12(16):2173–2185. doi:10.1002/smll.201502119
37. Cauda V, Engelke H, Sauer A, et al. Colchicine-loaded lipid bilayer-coated 50 nm mesoporous nanoparticles efficiently induce microtubule depolymerization upon cell uptake. *Nano Lett*. 2010;10(7):2484–2492. doi:10.1021/nl100991w
38. Rosenholm JM, Peuhu E, Bate-Eya LT, et al. Cancer-cell-specific induction of apoptosis using mesoporous silica nanoparticlesas drug-delivery vectors. *Small*. 2010;6(11):1234–1241. doi:10.1002/smll.200902355
39. Lin PY, Cheng YW, Chu CY, Chien KL, Lin CP, Tu YK. In-office treatment for dentin hypersensitivity: a systematic review and network meta-analysis. *J Clin Periodontol*. 2013;40(1):53–64. doi:10.1111/jcpe.12011
40. Bakry AS, Al-Hadeethi Y, Razvi MA. The durability of a hydroxyapatite paste used in decreasing the permeability of hypersensitive dentin. *J Dent*. 2016;51:1–7. doi:10.1016/j.jdent.2016.05.004
41. Yu J, Yang H, Li K, Lei J, Zhou L, Huang C. A novel application of nanohydroxyapatite/mesoporous silica biocomposite on treating dentin hypersensitivity: an in vitro study. *J Dent*. 2016;50:21–29. doi:10.1016/j.jdent.2016.04.005
42. Pei D, Meng Y, Li Y, Liu J, Lu Y. Influence of nano-hydroxyapatite containing desensitizing toothpastes on the sealing ability of dentinal tubules and bonding performance of self-etch adhesives. *J Mech Behav Biomed Mater*. 2019;91:38–44. doi:10.1016/j.jmbbm.2018.11.021
43. Niu LN, Zhang W, Pashley DH, et al. Biomimetic remineralization of dentin. *Dent Mater*. 2014;30(1):77–96. doi:10.1016/j.dental.2013.07.013
44. Al-Dulaijan YA, Weir MD, Melo MAS, et al. Protein-repellent nanocomposite with rechargeable calcium and phosphate for long-term ion release. *Dent Mater*. 2018;34(12):1735–1747. doi:10.1016/j.dental.2018.09.005
45. Liang K, Xiao S, Liu H, et al. 8DSS peptide induced effective dentinal tubule occlusion in vitro. *Dent Mater*. 2018;34(4):629–640. doi:10.1016/j.dental.2018.01.006
46. Feng Y, Zhong L, Hou Y, Jia S, Cui J. Acid-resistant enzyme@MOF nanocomposites with mesoporous silica shells for enzymatic applications in acidic environments. *J Biotechnol*. 2019;306:54–61. doi:10.1016/j.jbiotec.2019.09.010
47. Bossù M, Saccucci M, Salucci A, et al. Enamel remineralization and repair results of biomimetic hydroxyapatite toothpaste on deciduous teeth: an effective option to fluoride toothpaste. *J Nanobiotechnology*. 2019;17(1):17. doi:10.1186/s12951-019-0454-6
48. Kato MT, Leite AL, Hannas AR, et al. Impact of protease inhibitors on dentin matrix degradation by collagenase. *J Dent Res*. 2012;91(12):1119–1123. doi:10.1177/0022034512455801
49. Prati C, Montebugnoli L, Suppa P, Valdrè G, Mongiorgi R. Permeability and morphology of dentin after erosion induced by acidic drinks. *J Periodontol*. 2003;74(4):428–436. doi:10.1902/jop.2003.74.4.428
50. Wang Z, Jiang T, Sauro S, et al. Nerve-targeted desensitizing toothpastes occlude dentin tubules and induce mineral precipitation. *Am J Dent*. 2012;25(1):26–30.
51. Wierichs RJ, Stausberg S, Lausch J, Meyer-Lueckel H, Esteves-Oliveira M. Caries-preventive effect of NaF, NaF plus TCP, NaF plus CPP–ACP, and SDF varnishes on sound dentin and artificial dentin caries in vitro. *Caries Res*. 2018;52(3):199–211. doi:10.1159/000484483

52. Yang H, Pei D, Chen Z, Lei J, Zhou L, Huang C. Effects of the application sequence of calcium-containing desensitising pastes during etch-and-rinse adhesive restoration. *J Dent*. 2014;42(9):1115–1123. doi:10.1016/j.jdent.2014.03.018
53. Favretto CO, Delbem ACB, Moraes JCS, Camargo ER, de Toledo PTA, Pedrini D. Dentinal tubule obliteration using toothpastes containing sodium trimetaphosphate microparticles or nanoparticles. *Clin Oral Investig*. 2018;22(9):3021–3029. doi:10.1007/s00784-018-2384-3
54. Letchmanan K, Shen SC, Ng WK, et al. Mechanical properties and antibiotic release characteristics of poly(methyl methacrylate)-based bone cement formulated with mesoporous silica nanoparticles. *J Mech Behav Biomed Mater*. 2017;72:163–170. doi:10.1016/j.jmbbm.2017.05.003
55. Kind L, Stevanovic S, Wuttig S, et al. Biomimetic remineralization of carious lesions by self-assembling peptide. *J Dent Res*. 2017;96(7):790–797. doi:10.1177/0022034517698419
56. Bowen WH, Burne RA, Wu H, Koo H. Oral biofilms: pathogens, matrix, and polymicrobial interactions in microenvironments. *Trends Microbiol*. 2018;26(3):229–242. doi:10.1016/j.tim.2017.09.008
57. Xu X, Zhou XD, Wu CD. Tea Catechin epigallocatechin gallate inhibits streptococcus mutans biofilm formation by suppressing gtf genes. *Arch Oral Biol*. 2012;57(6):678–683. doi:10.1016/j.archoralbio.2011.10.021
58. Xu X, Zhou XD, Wu CD. The tea catechin epigallocatechin gallate suppresses cariogenic virulence factors of streptococcus mutans. *Antimicrob Agents Chemother*. 2011;55(3):1229–1236. doi:10.1128/AAC.01016-10
59. Tay FR, Pashley DH. Biomimetic remineralization of resin-ronded acid-etched dentin. *J Dent Res*. 2009;88(8):719–724. doi:10.1177/0022034509341826
60. Huang XQ, Camba J, Gu LS, et al. Mechanism of bioactive molecular extraction from mineralized dentin by calcium hydroxide and tricalcium silicate cement. *Dent Mater*. 2018;34(2):317–330. doi:10.1016/j.dental.2017.11.010
61. Kijsamanmith K, Banomyong D, Burrow MF, et al. Effect of conventional and acid-modified casein phosphopeptide-amorphous calcium phosphate crèmes on dentin permeability before and after acid challenge. *Oper Dent*. 2019;44(5):530–535. doi:10.2341/17-382-L
62. Dashper SG, Shen P, Sim CPC, et al. CPP-ACP promotes SnF efficacy in a polymicrobial caries model. *J Dent Res*. 2019;98(2):218–224. doi:10.1177/0022034518809088
63. Philip N, Leishman SJ, Bandara HMHN, Walsh LJ. Casein phosphopeptide-amorphous calcium phosphate attenuates virulence and modulates microbial ecology of saliva-derived polymicrobial biofilms. *Caries Res*. 2019;53(6):643–649. doi:10.1159/000499869
64. de Freitas RP, Greatti VR, Alcalde MP, et al. Effect of the association of nonsteroidal anti-inflammatory and antibiotic drugs on antibiofilm activity and pH of calcium hydroxide pastes. *J Endod*. 2017;43(1):131–134. doi:10.1016/j.joen.2016.09.014
65. Krämer N, Schmidt M, Lücker S, Domann E, Frankenberger R. Glass ionomer cement inhibits secondary caries in an in vitro biofilm model. *Clin Oral Investig*. 2018;22(2):1019–1031. doi:10.1007/s00784-017-2184-1
66. Wu J, Zhou C, Ruan J, et al. Self-healing adhesive with antibacterial activity in water-aging for 12 months. *Dent Mater*. 2019;35(8):1104–1116. doi:10.1016/j.dental.2019.05.004